Detection of a Dynamic Cone-Shaped Meniscus on the Surface of Fluids in Electric Fields

Ezinwa O. Elele,[1] Yueyang Shen,[1] Donald R. Pettit,[2] and Boris Khusid[1,*]
[1]New Jersey Institute of Technology, Newark, New Jersey 07102, USA
[2]NASA Johnson Space Center, Houston, Texas 77058, USA
(Received 13 September 2014; published 5 February 2015)

A cone-shaped meniscus of electrified fluids, often called a Taylor cone, is observed in rain drops and lightning and employed in various *physical instruments* and experimental techniques, but the way it evolves from a rounded shape to a cone is a long-standing puzzle. Earth's gravity and microgravity measurements on the meniscus whose height is just shy of droplet ejection reveal that field-driven cusp evolution exhibits a universal self-similarity insensitive to the forcing field and scaled by the fluid surface tension and density. Our work paves the way for dynamic control of field-driven phenomena in fluids.

DOI: 10.1103/PhysRevLett.114.054501 PACS numbers: 47.20.−k, 47.55.D−, 47.60.Kz, 47.65.−d

The conical meniscus of an electrified fluid with spontaneous sparks and fluid ejection has fascinated scientists for centuries [1–3]. This ubiquitous phenomenon is observed in rain drops and lightning and employed in electrospraying and ink jet printing [2,3], mass spectrometry [4,5], ion beam sources [6], plasma technology [7], fabrication of synthetic fibers [8,9], and nanostructures [10]. Taylor [11–13] showed that surface tension and electric forces form a steady-state conical meniscus with a semivertex angle of 49.3°. The initial loss of meniscus stability in a sufficiently strong field can be easily predicted by linear analysis [2,12]. However, field-driven meniscus evolution from a rounded shape to a cone is a long-standing puzzle in this well-studied phenomenon as it overlaps with spontaneous fluid ejection. In this Letter, we report data on the meniscus whose height is just shy of droplet ejection. Earth's gravity and microgravity measurements, spanning more than 2 orders of magnitude in length and time, reveal that field-driven cusp evolution exhibits a universal self-similarity insensitive to the forcing field while a 50% increase in applied voltage shortens the overall time for the meniscus to rise by more than an order of magnitude.

Until now, two types of apparatus pioneered in 1914–1931 by Zeleny [14–16], Wilson and Taylor [17], Nolan [18], and Macky [19] have been used to electrify fluids. In Refs. [14–17], voltage is applied to two bare electrodes, one immersed in the fluid and the other placed at a certain distance away from the fluid. In Refs. [18,19], a drop falls through or levitates in a field produced between two electrodes. The conditions of meniscus evolution and fluid ejection are similar in the apparatuses of both types. Spontaneous fluid ejection in these apparatuses effectively prevents the study of cusp dynamics. The apparatus in Fig. 1 was designed to create and control a cone-shaped meniscus by limiting the buildup of an electric charge on its surface and thus allowing a dynamic regime to be investigated without drop ejection. This is achieved by separating a drop from the ground electrode with an electrically insulating film that does not allow electric current to flow between the electrodes (item 4 in Fig. 1). Because of the film presence, the drop serves as a floating electrode capacitively coupled to the electrodes (items 2 and 5 in Fig. 1). Details of the setup are listed in the Supplemental Material [20]. The energized electrode is a metal tube fitted on an insulating nozzle 0.2 mm above the nozzle exit. A drop is ejected through the nozzle onto the insulating film. The distance between the drop apex and the nozzle exit is set to 0.6 mm. As the electric stress exerted on a fluid is proportional to the square of the field strength, a field is generated by a train of rectangular voltage pulses of oscillating polarity (slew rate 0.75 kV/μs) to keep the electric stress at a constant level similar to classical experiments [11–19] but reduce the accumulation of charge on the drop surface due to the voltage reversals.

Experiments were conducted over a wide range of fluid properties (see the Supplemental Material [20], Table 1): density $\rho \sim 1$ g/cm^3, viscosity $\eta \sim 1$–76 cP, conductivity $\sigma \sim 0.02$–10^4 μS/cm, dielectric constant $\varepsilon \sim 2.7$–90,

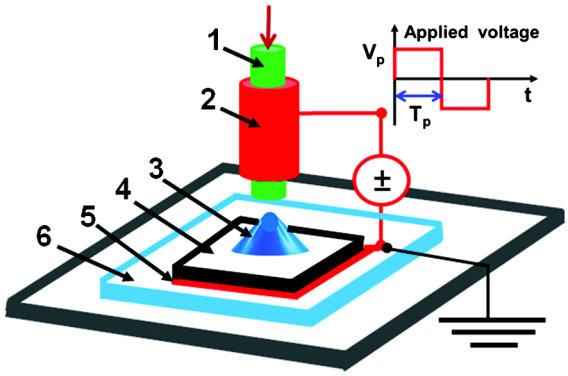

FIG. 1 (color online). Concept of experimental apparatus. 1, Electrically insulating nozzle; 2, energized electrode; 3, drop; 4, insulating film; 5, ground electrode; 6, insulating cover of 3D movable stage; V_p, pulse voltage; T_p, time of reversing voltage polarity.

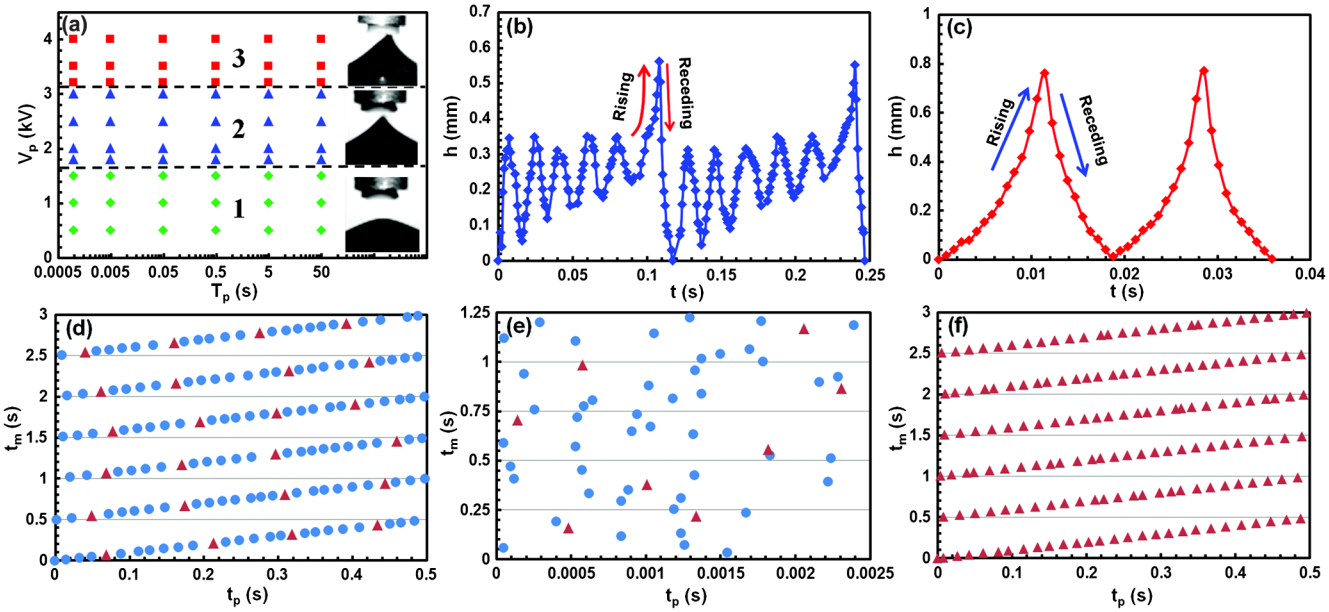

FIG. 2 (color online). Deionized water. Earth's gravity experiments on 10-μL drop. (a) V_p-T_p diagram for modes 1, 2, 3 of drop evolution. Photos illustrate drop behavior. (b),(c) Displacement h of drop apex as a function of time t in mode 2 at $T_p = 0.5$ s and $V_p =$ (b) 2 kV, (c) 3 kV. Cones appear in rising at $h =$ (b) 0.32 ± 0.03 mm, (c) 0.22 ± 0.02 mm. Larger h at 3 kV caused by drop spreading. (d),(e),(f) Mode 2. Time instance t_m when the drop apex reaches its maximum displacement h_m vs time t_p passed after the last voltage polarity reversal; circles and triangles refer to rounded and pointed ends. $V_p/T_p =$ (d) 2 kV/0.5 s, (e) 2 kV/2.5 ms, (f) 3 kV/0.5 s.

surface tension $\gamma \sim 30$–72 dyn/cm, contact angle on the insulating film (item 4 in Fig. 1) $\theta \sim 9$–$56°$, charge relaxation time $t_e = \varepsilon\varepsilon_0/\sigma \sim 1$ ns–13 μs with the vacuum permittivity ε_0. The fluids as numbered in all figures were (1) deionized (DI) water, (2) DI water with 0.1M KCl, (3) polyethylene glycol PEG 200, (4) polymer solution simulating human saliva, and (5) low-conducting lubricant with 0.02 wt % graphene. The application of high-voltage pulses to a drop of pure lubricant caused the meniscus to oscillate but did not produce a pointed protrusion. As the lubricant conductivity was increased by adding graphene flakes, a drop formed a cone-shaped meniscus. Measurements under microgravity (1.5 μg) on the International Space Station (ISS) allowed length scales to be expanded from the submillimeter to the centimeter range.

Depending on the pulse voltage V_p and length T_p (Fig. 1), three modes of meniscus evolution were observed under Earth's gravity [Fig. 2(a) for DI water and similar for other fluids]. Mode 1 occurs when the electric force is weak compared with the capillary and gravity forces. The fluid level rises to form a stationary bell-shaped hump in the high field region under the nozzle. When V_p exceeds the instability threshold, the portion of the fluid meniscus under the nozzle rises, oscillatory or monotonically for larger voltage and fluid viscosity, and produces a pointed protrusion. The threshold field ~2 kV/mm is similar to the value observed in conventional apparatuses [12,23].

Mode 2, the subject of this work and referred to as the dynamic Taylor cone, is attributed to voltages forming a cone-shaped meniscus that rises to a certain height, recedes, and then repeats itself again and again. Remarkably, meniscus evolution of low volatile PEG 200 drop, Fig. 3(a), does not change throughout 8 h testing (1.8×10^5 oscillations). The overall time for the meniscus to rise is governed by the pulse voltage. The increase of V_p from 2 to 3 kV shortens it by more than an order of magnitude [Figs. 2(b) and 2(c) for DI water and similar for other fluids]. As the frequency in varying the pulse polarity increases, meniscus oscillations gradually become more irregular since a change in the voltage polarity disturbs the drop by reversing the sign of the charge induced on the fluid surface. To graphically display the effects of disturbances, we plot a series of consecutive time instances t_m in which the drop apex rises to maximum height h_m against the amount of time t_p that passed in each such instance after the last change in the pulse polarity [Figs. 2(d)–2(f) for DI water and similar for other fluids]. Meniscus oscillations at a fixed pulse polarity $0 < t_p < T_p$ are represented on this diagram with a set of neighboring points in the direction of increasing t_p. Patterns of well-ordered points demonstrate periodicity of cone-shaped tips formed at long pulses, whereas randomly scattered points show irregular cone formation at short pulses. However, a cone is remarkably insensitive to disturbances and, once formed, evolves in the same way, Fig. 3(b).

Mode 3 occurs for larger voltages. The meniscus develops a cone-shaped tip, ejects droplets and then recedes. The

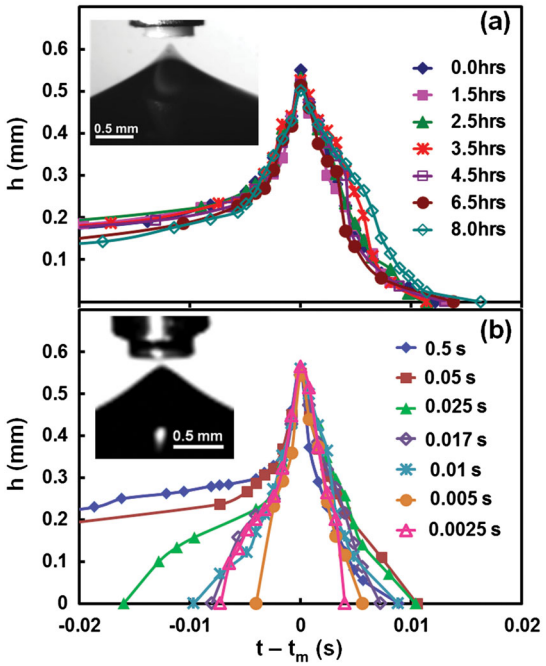

FIG. 3 (color online). Earth's gravity experiments. Displacement h of 10-μL drop apex as a function of time t-t_m, t_m is the instance of rising to maximum h_m. (a) Meniscus evolution of low volatile PEG 200 drop throughout 8 h testing at $V_p/T_p = 2\,\mathrm{kV}/0.5\,\mathrm{s}$. Cones appear at $0 > t\text{-}t_m > -3.0 \pm 0.21$ ms, $h > 0.31 \pm 0.02$ mm. Symbols refer to testing time. Photo at 8 h. (b) Polymer solution simulating human saliva forms cones at $0 > t\text{-}t_m > -1.67 \pm 0.15$ ms, $h > 0.32 \pm 0.02$ mm for $V_p = 2$ kV. Symbols refer to time of changing voltage polarity T_p. Cones form sporadically at $T_p = 5$ and 2.5 ms and periodically at longer T_p. Photo at $T_p = 2.5$ ms.

process repeats itself several times and rapidly comes to an end when the drop volume becomes depleted. As the air dielectric strength ~3 kV/mm, it begins to break down over a rising pointed protrusion in modes 2 and 3 and becomes partially conducting. In mode 2, a conducting channel bridges the air gap earlier than the meniscus ejects fluid. Once it forms, buildup of charge on the insulating film under the drop (item 4 in Fig. 1) reduces the field strength in the gap and chokes the electric current flow similar to that in the dielectric-barrier discharge in air [24,25]. The charge transferred through the air gap produces a low current (estimated ~nA); thus, no light emissions or sparks were observed. Self-arresting of fluid ejection in mode 2 is achieved by designing the electrical capacitance between the drop and the ground electrode to be much larger than the capacitance between the drop and the energized electrode. The voltage across the air gap therefore prevails when a pointed protrusion rises but reduces drastically as a discharge occurs.

Microgravity experiments on DI-water drops of several centimeters in size were carried out aboard ISS in Expedition 30/31. Voltage was produced with a belts-and-rollers type Van de Graaff generator assembled from LEGOs (details in the Supplemental Material [20]). Water placed on the 9.8-cm diameter collector sphere formed a cone-shaped meniscus when another drop situated on an electrically insulating support was brought nearby to serve as a floating electrode for increasing the local field (photos in Figs. 4,5). Three modes of meniscus evolution that appeared in Earth's gravity experiments were observed on ISS. Similar to the apparatus in Fig. 1, buildup of charge on the insulating support choked the electric current between the drops when a discharge occurred. A cone-shaped tip formed by a drop either emitted some fluid or receded if charge leakage weakened the electric force. Observations of microgravity dynamic Taylor cones in mode 2 are presented here.

The exceptional robustness of mode 2 made it possible to study the cusp evolution over a broad range of length and time scales. As a protrusion develops, its round top shrinks approaching the cone shape. The limiting value of its semivertex angle averaged over all data under Earth's gravity is $48.3° \pm 1.7°$, and $46.8° \pm 2.4°$ under microgravity that is close to the Taylor angle 49.3° [11]. Displacement of the drop apex h is plotted in Fig. 4 over the time period of the constant vertex angle. This log-log plot demonstrates the power-law scaling over 2 orders of magnitude in length and time with the slope 0.64 ± 0.04 remarkably close to 2/3 recently observed in computer simulations [26,27] of the cone rise. The slope changes to 0.42 in the mode 3 regime when a cone-shaped tip ejects droplets [28]. Starting with the 2/3 power law, we can form a dimensionless parameter

$$\xi = (h_m - h)/[\gamma(t_m - t)^2/\rho]^{1/3} \qquad (1)$$

that measures the cusp self-similarity before the singularity. All Earth's and microgravity measurements in Fig. 4

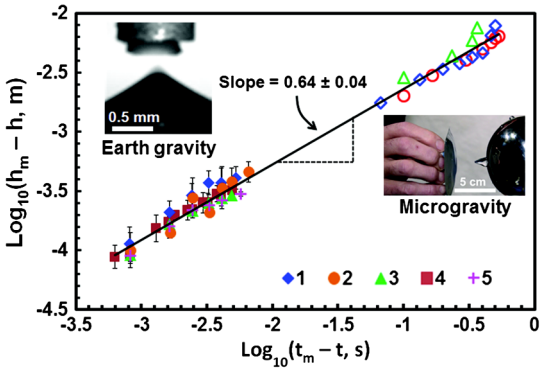

FIG. 4 (color online). Dynamic Taylor cone. Displacement h of drop apex as a function of time $t_m - t$, t_m is the instance of rising to maximum h_m. Filled symbols refer to experiments under Earth's gravity on 10-μL drops at $V_p = 2$ and 3 kV with $T_p = 0.5$ s. Data and error bars from 20 randomly chosen videos of three drops for each fluid. Open symbols refer to data under microgravity on three 0.5-mL DI-water drops. Photos show DI-water drops.

collapse on a value of $\xi = 0.30 \pm 0.05$. The meniscus semivertex angle θ and ξ converge gradually to their limiting values as h approaches h_m regardless of the drop volume, voltage, and gravity, even though ξ monotonically increases for small drops and decreases for large drops (Fig. 5). Scaling of the instantaneous meniscus shape, relative height $H(r,t)$ vs radius r, with the instantaneous distance of the tip from its maximum $h_m - h = H(0,t)$ demonstrates the universal self-similarity of cusp evolution (Fig. 5). The self-similarity of field-induced cusp evolution appears to be independent
of the forcing field and surprisingly resembles self-similarity observed in breakup of liquid drops, sheets, and eruption of jets in the absence of a field [3,29–32] when the surface tension and inertial forces dominate.

Now we present a scaling analysis of meniscus evolution. Relative contributions of the gravity, viscous, electric, and surface tension forces in its initial stage are represented [2,3] by the gravity Bond number $\mathrm{Bo}_g = \rho g R_D^2/\gamma$, the Ohnesorge number $\mathrm{Oh} = \eta/\sqrt{\rho R_D \gamma}$, and the pulse electric Bond number $\mathrm{Bo}_e = \varepsilon_0 E_{\mathrm{ext}}^2 R_D/2\gamma$ with the gravitational acceleration g, the drop diameter $2R_D$, and the external field strength estimated as $E_{\mathrm{ext}} = V_p/S$, where S is the separation between the energized electrode and the drop apex (Fig. 1). Mode 2 was observed at $\mathrm{Bo}_g \sim 0.04$–0.08, $\mathrm{Oh} \sim 0.005$–0.48, $\mathrm{Bo}_e \sim 0.2$–1 in Earth's gravity and $\mathrm{Bo}_g < \sim 10^{-4}$, $\mathrm{Oh} \sim 10^{-3}$, $\mathrm{Bo}_e \sim 2.7$–6.5 in microgravity [20] when the electric, inertial, and surface tension forces dominated. The self-similar cusp evolution described by Eq. (1) with $\xi \approx 0.3$ is not affected by the fluid viscosity as it occurs at h_m-h and t_m-t (Figs. 4,5) much greater than the viscous length $L_\eta = \eta^2/\gamma\rho$ and time $t_\eta = \eta^3/\gamma^2\rho$ scales where viscous forces are important [3]: $L_\eta \sim 0.014$–119 μm, $t_\eta \sim 0.0002$–206 μs for tested fluids (see the Supplemental Material [20], Table 1). Relative contributions of inertia and surface tension to unsteady flow are represented by the Weber number $\mathrm{We} = \rho v^2 L/\gamma$ measuring the ratio of the fluid kinetic energy to its surface energy [3] and the ratio of the fluid acceleration force to the surface tension force $A = \rho L^2 dv/dt/\gamma$, where L and v are the characteristic length and velocity. Taking h_m-h and dh/dt from Eq. (1) with $\xi \approx 0.3$ for L and v in the cusp region whose radial and longitudinal scales are of the same order (Fig. 5), we obtain $\mathrm{We} = 2A \sim 0.012$. Since the viscous and inertial forces are relatively small, the capillary and electric pressures are nearly balanced in the cusp region. Therefore, the field in air at the cusp surface can be approximated by Taylor's solution for a cone in equilibrium $E_a \sim \sqrt{2\gamma/\varepsilon_0 R}$ [11] with the radius of cusp curvature R scaled with h_m-h (Fig. 5). The cusp charge increases with decreasing h_m-h. To estimate the field E_f in fluid, we use the balance equation for charge transport to the cusp surface by conduction $\varepsilon_0 d(E_a - \varepsilon E_f)/dt = \sigma E_f$ that yields $E_f/E_a \sim t_e/(t_m - t) \ll 1$ as the charge relaxation time t_e is shorter by several orders of magnitude than the period of cusp motion (Fig. 4). Since E_f is negligible, the field around the cusp is well approximated by Taylor's solution for an equipotential cone in equilibrium [11] that yields the limiting value of the semivertex cusp angle close to 49.3° (Fig. 5). As $E_a \gg E_{\mathrm{ext}}$ in the range of h_m-h, where $\xi \approx 0.3$ (Figs. 4,5), cusp motion is not affected by applied voltage. In fact, scaling of the instantaneous cusp shape given by Fig. 5 and Eq. (1) represents the self-similar solution of electrohydrodynamic equations for an inviscid conducting fluid with the electric pressure scaled by the capillary pressure.

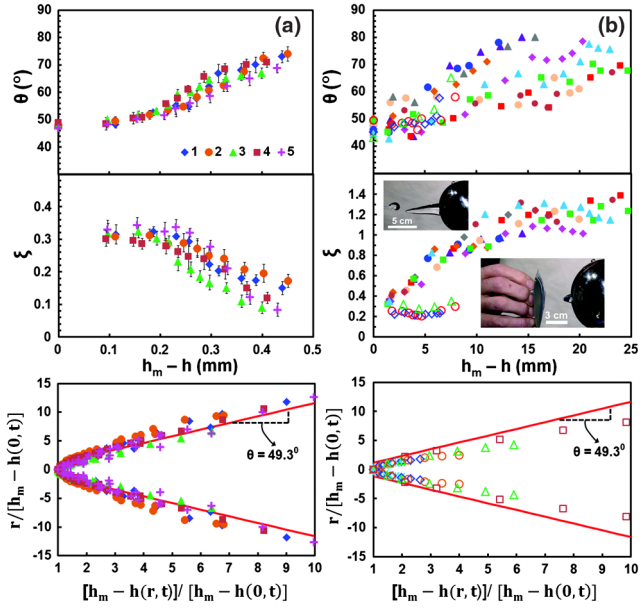

FIG. 5 (color online). Meniscus rising in mode 2. Semivertex angle θ and parameter ξ as a function of h_m-h, and the instantaneous meniscus shape scaled with the instantaneous distance of the tip from its maximum h_m-h. (a) Experiments under Earth's gravity on 10-μL drops at $V_p = 2$ and 3 kV with $T_p = 0.5$ s. Data and error bars for θ, ξ from 10 randomly chosen videos of three drops for each fluid; six instantaneous shapes of a drop at 2 kV used to construct the scaled meniscus shape. (b) Experiments under microgravity on DI-water drops. Filled and open symbols refer to ten 10-mL drops (top photo) and three 0.5-mL drops (bottom photo); five instantaneous shapes of a 0.5-mL drop used to construct the scaled meniscus shape.

The cusp evolution generates a vortex flow that can affect mixing and separation processes in the drop (Supplemental Material [20], Fig. 1). Examples are shown in the Supplemental Material, Fig. 2(a), where polystyrene spheres are concentrated under the conical apex or dispersed, and Supplemental Material, Fig. 2(b) [20], where gypsum rapidly precipitates from a supersaturated aqueous solution.

In summary, we have revealed the universal self-similarity of the field-induced meniscus evolution from a rounded shape to a cone that is scaled by the fluid surface

tension and density. The proposed noncontact technique paves the way for dynamic control of field-driven phenomena in widespread applications [2–10,33].

We are thankful to Andreas Acrivos, Osman A. Basaran, and Paul H. Steen for stimulating discussions and comments on the interpretation of experimental data. Research funded by National Aeronautics and Space Administration Grants No. NNX09AK06G and No. NNX13AQ53G.

*khusid@njit.edu

[1] J. L. Heilbron, *Electricity in the 17th and 18th Century: A Study of Early Modern Physics* (University of California Press, Berkley, 1979).
[2] J. Fernandez de la Mora, The fluid dynamics of Taylor cones, Annu. Rev. Fluid Mech. **39**, 217 (2007).
[3] J. Eggers and E. Villermaux, Physics of liquid jets, Rep. Prog. Phys. **71**, 036601 (2008).
[4] J. B. Fenn, M. Mann, C. K. Meng, S. F. Wong, and C. M. Whitehouse, Electrospray ionization: Principles and practice, Mass Spectrom. Rev. **9**, 37 (1990).
[5] M. Wilm, A. Shevchenko, T. Houthaeve, S. Breit, L. Schweigerer, T. Fotsis, and M. Mann, Femtomole sequencing of proteins from polyacrylamide by nano-electrospray mass spectrometry, Nature (London) **379**, 466 (1996).
[6] J. Gierak, Focused ion beam technology and ultimate applications, Semicond. Sci. Technol. **24**, 043001 (2009).
[7] P. Bruggeman and C. Leys, Non-thermal plasmas in and in contact with liquids, J. Phys. D **42**, 053001 (2009).
[8] R. Langer and D. A. Tirrell, Designing materials for biology and medicine, Nature (London) **428**, 487 (2004).
[9] D. H. Reneker and A. L. Yarin, Electrospinning jets and polymer nanofibers, Polymer **49**, 2387 (2008).
[10] S. Matsui and Y. Ochiai, Focused ion beam applications to solid state devices, Nanotechnology **7**, 247 (1996).
[11] G. I. Taylor, Disintegration of water drops in an electric field, Proc. R. Soc. A **280**, 383 (1964).
[12] G. I. Taylor and A. D. McEwan, The stability of a horizontal fluid interface in a vertical electric field, J. Fluid Mech. **22**, 1 (1965).
[13] G. I. Taylor, Electrically driven jets, Proc. R. Soc. A **313**, 453 (1969).
[14] J. Zeleny, The electrical discharge from liquid points and a hydrostatic method of measuring the electric intensity at their surfaces, Phys. Rev. **3**, 69 (1914).
[15] J. Zeleny, On the conditions of instability of electrified drops with applications to the electrical discharge from liquid points, Proc. Cambridge Philos. Soc. **18**, 71 (1915).
[16] J. Zeleny, Instability of electrified liquid surfaces, Phys. Rev. **10**, 1 (1917).
[17] C. T. R. Wilson and G. I. Taylor, The bursting of soap-bubbles in a uniform electric field, Math. Proc. Cambridge Philos. Soc. **22**, 728 (1925).
[18] J. J. Nolan, The breaking of water drops by electric fields, Proc. R. Irish Acad., Sect. A **37**, 28 (1926).
[19] W. A. Macky, Some investigations on the deformation and breaking of water drops in strong electric fields, Proc. R. Soc. A **133**, 565 (1931).
[20] See Supplemental Material at http://link.aps.org/supplemental/10.1103/PhysRevLett.114.054501, which includes Refs. [21,22], for (S1) experimental setups, (S2) fluid properties, and (S3) additional experimental data.
[21] E. Kuffel, W. S. Zaengl, and J. Kuffe, *High Voltage Engineering. Fundamentals*, 2nd ed. (Elsevier, Oxford, 2000).
[22] D.-J. Oh, J.-Y. Lee, Y.-K. Kim, and H.-S. Kho, Effects of carboxymethylcellulose (CMC)-based artificial saliva in patients with xerostomia, Int. J. Oral Maxillofac. Surg. **37**, 1027 (2008).
[23] P. Bruggeman, L. Graham, J. Degroote, J. Vierendeels, and C. Leys, Water surface deformation in strong electrical fields and its influence on electrical breakdown in a metal pin-water electrode system, J. Phys. D **40**, 4779 (2007).
[24] U. Kogelschatz, Dielectric-barrier discharges: Their history, discharge physics, and industrial applications, Plasma Chem. Plasma Process. **23**, 1 (2003).
[25] A. Fridman, A. Chirokov, and A. Gutsol, Non-thermal atmospheric pressure discharges, J. Phys. D **38**, R1 (2005).
[26] V. G. Suvorov and N. M. Zubarev, Formation of the Taylor cone on the surface of liquid metal in the presence of an electric field, J. Phys. D **37**, 289 (2004)
[27] J. C. Burton and P. Taborek, Simulations of Coulombic Fission of Charged Inviscid Drops, Phys. Rev. Lett. **106**, 144501 (2011).
[28] L. Oddershede and S. R. Nagel, Singularity during the Onset of an Electrohydrodynamic Spout, Phys. Rev. Lett. **85**, 1234 (2000).
[29] A. U. Chen, P. K. Notz, and O. A. Basaran, Computational and Experimental Analysis of Pinch-Off and Scaling, Phys. Rev. Lett. **88**, 174501 (2002).
[30] Y. I. Chen and P. H. Steen, Dynamics of inviscid capillary breakup: Collapse and pinchoff of a film bridge, J. Fluid Mech. **341**, 245 (1997).
[31] R. F. Day, E. J. Hinch, and J. R. Lister, Self-Similar Capillary Pinchoff of an Inviscid Fluid, Phys. Rev. Lett. **80**, 704 (1998).
[32] B. W. Zeff, B. Kleber, J. Fineberg, and D. P. Lathrop, Singularity dynamics in curvature collapse and jet eruption on a fluid surface, Nature (London) **403**, 401 (2000).
[33] K. Choi, A. H. C. Ng, R. Fobel, and A. R. Wheeler, Digital microfluidics, Annu. Rev. Anal. Chem. **5**, 413 (2012).